Surface Tension and Energy in Multivariant Martensitic Transformations: Phase-Field Theory, Simulations, and Model of Coherent Interface

Valery I. Levitas[1] and Mahdi Javanbakht[2]

[1]*Iowa State University, Departments of Mechanical Engineering, Aerospace Engineering, and Material Science and Engineering, Ames, Iowa 50011, USA*

[2]*Iowa State University, Department of Mechanical Engineering, Ames, Iowa 50011, USA*

(Received 5 June 2010; revised manuscript received 9 September 2010; published 12 October 2010)

The Ginzburg-Landau theory for multivariant martensitic phase transformations is advanced in three directions: the potential is developed that introduces the surface tension at interfaces; a mixed term in gradient energy is introduced to control the martensite-martensite interface energy independent of that for austenite-martensite; and a noncontradictory expression for variable surface energy is suggested. The problems of surface-induced pretransformation, barrierless multivariant nucleation, and the growth of an embryo in a nanosize sample are solved to elucidate the effect of the above contributions. The obtained results represent an advanced model for coherent interface.

DOI: 10.1103/PhysRevLett.105.165701 PACS numbers: 64.60.Bd, 63.70.+h, 64.60.an

Phase-field or Ginzburg-Landau (GL) modeling represents a unique approach for simulation of various aspects of stress-induced multivariant martensitic phase transformations (PTs) [1]. Recently [2], we developed a much more sophisticated Landau potential to make the theory conceptually consistent with known experimental data for shape-memory alloys, steel, and ceramics. The athermal resistance to interface motion is introduced [3], and the theory is extended for large strain [4], dynamics [5], and microscale [6]. In these approaches and below, each of the n-order parameters η_i varies from 0 (corresponding to A) to 1 (corresponding to martensitic variant M_i). This Letter advances the GL approach in three directions. (a) Since the thickness of martensitic variants is of the order of 1 nm and they possess sharp tips, surface tension should play a significant role. However, we are not aware of any publications on this topic. We introduce proper terms in the energy potential, resulting in an expression for the surface tension for multivariant PTs that are thermodynamically consistent and consistent with a sharp-interface limit. The nontrivial points in this consideration are that even for negligible small strains we have to use a large strain formulation, consider the gradient of the order parameters with respect to a deformed configuration, and introduce the ratio of mass densities in the nondeformed and deformed states ρ_0/ρ in some terms. Note that even for liquid-liquid and liquid-solid interfaces, for which expressions for surface tension have been known for decades, they are not completely consistent with a sharp-interface limit because they result in additional hydrostatic pressure [7]. Inconsistency with a sharp-interface approach means that a theory contains internal contradictions. We resolved this problem for these interfaces as well. (b) Differences in the surface energies of different phases result in surface-induced phenomena—e.g., surface premelting, ordering or disordering [8]—however, it was not considered for martensitic PTs. The main drawback of previous works is that the utilized expression for surface energy $q(\eta) = a + b\eta^2$ does not allow for a homogeneous solution for the product phase—i.e., the product phase always has a surface structure toward the alternative phase, even when this phase is completely unstable. Here, we derive the expression for $q(\eta)$ that does not possess the above problems, generalize it for multivariant PTs, and study surface-induced pretransformation and barrierless nucleation of multiple martensitic variants. (c) The current form of the gradient energy results in the energy E_{MM} of the $\mathsf{M}_i - \mathsf{M}_j$ interface to be twice of energy E_{AM} of $\mathsf{A} - \mathsf{M}_i$ interface (see below), while in reality it is independent of the energy of the $\mathsf{A} - \mathsf{M}_i$ interface and is significantly smaller. We generalize the expression for gradient energy by introducing the products $\nabla\eta_i \cdot \nabla\eta_j$ in order to be able to control the energy of $\mathsf{M}_i - \mathsf{M}_j$ interface independently.

Combining all of the above advancements, the coupled system of time-dependent GL equations for all order parameters, the continuum mechanical equations, and the boundary conditions are formulated. The finite element method (FEM) approach, algorithm, and subroutines are developed using the COMSOL code. Model problems of surface-induced pretransformation, barrierless multivariant nucleation, and nanostructure evolution in a nanosize sample are solved, and the effect of the above contributions is elucidated. The obtained results represent a more detailed, flexible, and precise model for coherent solid-solid interface than current phenomenological models [9].

We designate contractions of tensors over one and two indices as $\boldsymbol{A} \cdot \boldsymbol{B} = \{A_{ij}B_{jk}\}$ and $\boldsymbol{A}{:}\boldsymbol{B} = A_{ij}B_{ji}$, respectively. The subscripts s, e, and t mean symmetrization and elastic and transformational strains; $\boldsymbol{I}$ is the unit tensor; $\mathring{\nabla}$ and ∇ are the gradient operators in the undeformed and deformed states; and $\otimes$ is a dyadic product.

Model.—Let us define the Helmholtz free energy per unit undeformed volume $\psi = \psi(\boldsymbol{B}, \eta_i, \boldsymbol{\nabla}\eta_i, \theta)$, where $\boldsymbol{B} = 0.5(\boldsymbol{V}\cdot\boldsymbol{V} - \boldsymbol{I})$ is the finite strain measure, $\boldsymbol{V}$ is the left stretch tensor, and θ is the temperature. Traditional thermodynamic procedure for the thermodynamic potential depending on $\boldsymbol{\nabla}\eta_i$ and linear relationships between thermodynamic forces and fluxes leads to

$$\boldsymbol{\sigma} = \frac{\rho}{\rho_0}\boldsymbol{V}\cdot\frac{\partial\psi}{\partial\boldsymbol{B}}\cdot\boldsymbol{V} - \sum_{i=1}^{n}\frac{\rho}{\rho_0}\left(\boldsymbol{\nabla}\eta_i\otimes\frac{\partial\psi}{\partial\boldsymbol{\nabla}\eta_i}\right)_s;$$
$$\frac{1}{L}\frac{\partial\eta_i}{\partial t} = -\frac{\rho}{\rho_0}\frac{\partial\psi}{\partial\eta_i}\Big|_{\boldsymbol{B}} + \boldsymbol{\nabla}\cdot\left(\frac{\rho}{\rho_0}\frac{\partial\psi}{\partial\boldsymbol{\nabla}\eta_i}\right), \tag{1}$$

where L is the kinetic coefficient, $\boldsymbol{\sigma}$ is the true Cauchy stress tensor, and $\partial\psi/\partial\eta_i$ is calculated at $\boldsymbol{B} = \text{const}$. While theory was developed for large strains similar to [4], to make it more accessible we simplify it for small elastic and shear transformation strains and rotations but keep finite volumetric transformation strains, where necessary. This is the minimum requirement for the correct introduction of surface tension. For this case, $\boldsymbol{\epsilon} = (\mathring{\boldsymbol{\nabla}}\boldsymbol{u})_s$, $\boldsymbol{\epsilon} = \boldsymbol{\epsilon}_e + \boldsymbol{\epsilon}_t$, where $\boldsymbol{u}$ is displacement, $\boldsymbol{\epsilon} = 1/3\varepsilon_0\boldsymbol{I} + \boldsymbol{e}$ is the total strain tensor, and ε_0 and $\boldsymbol{e}$ are the volumetric and deviatoric contributions to strain. Also, for simplicity we assume that ψ is an isotropic function of $\boldsymbol{\epsilon}_e$ and $\boldsymbol{\nabla}\eta_i$, $\psi = \bar{\psi}(\boldsymbol{\epsilon}_e, \eta_i, \theta, \boldsymbol{\nabla}\eta_i)$. Functions ψ and $\boldsymbol{\epsilon}_t$ are accepted in the form

$$\psi = \psi^e(\varepsilon_0, \boldsymbol{e}, \eta_i, \theta) + \underline{\frac{\rho_0}{\rho}}\breve{\psi}^\theta + \psi^\theta + \underline{\frac{\rho_0}{\rho}}\psi^\nabla;$$
$$\psi^\theta = \sum_{k=1}^{n}\frac{1}{3}A_0(\theta-\theta_e)\eta_k^2(3-2\eta_k) - \sum_{i=1}^{n-1}\sum_{j=i+1}^{n}\eta_i^2\eta_j^2(\eta_i+\eta_j)A_0(\theta-\theta_e); \tag{2}$$

$$\psi^\nabla = \frac{\beta}{2}\left(\sum_{i=1}^{n}|\boldsymbol{\nabla}\eta_i|^2 + \underline{b\sum_{i=1}^{n}\sum_{j=1,i\neq j}^{n}\boldsymbol{\nabla}\eta_i\cdot\boldsymbol{\nabla}\eta_j}\right); \tag{3}$$

$$\breve{\psi}^\theta = \sum_{k=1}^{n}A_0(\theta_e-\theta_c)\eta_k^2(1-\eta_k)^2 + \sum_{i=1}^{n-1}\sum_{j=i+1}^{n}F_{ij}(\eta_i,\eta_j); \tag{4}$$

$$\boldsymbol{\epsilon}_t = \sum_{k=1}^{n}\boldsymbol{\epsilon}_t^k[a\eta_k^2 + (4-2a)\eta_k^3 + (a-3)\eta_k^4] - \sum_{i=1}^{n-1}\sum_{j=i+1}^{n}\eta_i^2\eta_j^2(\eta_i\boldsymbol{L}_{ij} + \eta_j\boldsymbol{L}_{ji}), \tag{5}$$

Here, $\frac{\rho_0}{\rho} = 1+\varepsilon_0$, $\boldsymbol{L}_{ij} = (a-3)\boldsymbol{\epsilon}_t^j + 3\boldsymbol{\epsilon}_t^i$, $F_{ij}(\eta_i,\eta_j) = \eta_i\eta_j(1-\eta_i-\eta_j)\{B[(\eta_i-\eta_j)^2-\eta_i-\eta_j] + C\eta_i\eta_j\} + \eta_i^2\eta_j^2(\eta_i+\eta_j)[\bar{A} - A_0(\theta_e-\theta_c)]$, $\psi^e = \frac{1}{2}K\varepsilon_{0e}^2 + \frac{1}{2}\mu\boldsymbol{e}_e{:}\boldsymbol{e}_e$ is the elastic energy with equal (for compactness) bulk K and shear μ moduli; θ_e and θ_c are the equilibrium temperature and temperature for the loss of stability of A; $\boldsymbol{\epsilon}_{ti}$ is the transformation strains of the ith variant; $i=0$ corresponds to A; β, A_0, $\bar{A}$, B, C, a, and b are parameters. Then Eq. (1) looks like

$$\boldsymbol{\sigma} = \boldsymbol{\sigma}_e + \boldsymbol{\sigma}_{\text{st}};$$
$$\boldsymbol{\sigma}_e = \frac{\partial\psi}{\partial\varepsilon_0}\boldsymbol{I} + \frac{1}{(1+\varepsilon_0)^{2/3}}\frac{\partial\psi}{\partial\boldsymbol{e}} = K\varepsilon_{0e}\boldsymbol{I} + \frac{\mu}{(1+\varepsilon_0)^{2/3}}\boldsymbol{e}_e; \tag{6}$$

$$\boldsymbol{\sigma}_{\text{st}} = (\psi^\nabla + \breve{\psi}_\theta)\boldsymbol{I} - \beta\sum_{i=1}^{n}(\boldsymbol{\nabla}\eta_i\otimes\boldsymbol{\nabla}\eta_i + b\boldsymbol{\nabla}\eta_i\otimes\sum_{j=1,i\neq j}^{n}\boldsymbol{\nabla}\eta_j); \tag{7}$$

$$\frac{1}{L}\frac{\partial\eta_i}{\partial t} = \frac{\rho}{\rho_0}(K\varepsilon_{0e}\boldsymbol{I} + \mu\boldsymbol{e}_e){:}\frac{d\boldsymbol{\epsilon}_t}{d\eta_i} - \frac{\rho}{\rho_0}\frac{\partial\psi^\theta}{\partial\eta_i} - \frac{\partial\breve{\psi}^\theta}{\partial\eta_i} + \beta(\boldsymbol{\nabla}^2\eta_i + b\sum_{j=1,i\neq j}^{n}\boldsymbol{\nabla}^2\eta_j), \tag{8}$$

where $\boldsymbol{\sigma}_{\text{st}}$ is the surface tension. For a single order parameter (e.g., for liquid-liquid interfaces) and a phase equilibrium condition, $\frac{\beta}{2}|\boldsymbol{\nabla}\eta|^2 = \breve{\psi}_\theta$ [2], and we have

$$\boldsymbol{\sigma}_{\text{st}} = \beta|\boldsymbol{\nabla}\eta|^2(\boldsymbol{I} - \boldsymbol{k}\otimes\boldsymbol{k}); \qquad \boldsymbol{k} = \boldsymbol{\nabla}\eta/|\boldsymbol{\nabla}\eta|. \tag{9}$$

Here, $\boldsymbol{k}$ is the unit normal to the interface. Thus, $\boldsymbol{\sigma}_{\text{st}}$ represents two equal normal stresses acting along the interface, i.e., like surface tension in the sharp-interface approach, in contrast to [7]. Since $\beta|\boldsymbol{\nabla}\eta|^2$ is the total η-related energy, its integration along the $\boldsymbol{k}$ gives the total interface energy, such as for sharp-interface.

Let us discuss obtained equations. The main difference between the current and our previous formulation for energy Eq. (2) [2,4] is in the underlined terms and in using the gradient operator $\boldsymbol{\nabla}$ with respect to the deformed state. When $\rho_0 \simeq \rho$, $b = 0$, and $\boldsymbol{\nabla} \simeq \mathring{\boldsymbol{\nabla}}$, ψ is equivalent to that in [2,4]. It looks like it is not a significant change, but that is exactly what is necessary (excluding $b \neq 0$) to introduce surface tension for martensitic PT and to make it consistent with a sharp-interface approach. The nontriviality of the results is related to the fact that for small strain it is customary to assume that $\rho_0 \simeq \rho$ and $\boldsymbol{\nabla} \simeq \mathring{\boldsymbol{\nabla}}$. However, this results in $\boldsymbol{\sigma}_{\text{st}} = 0$. The point is that even for absolutely negligible strain $d(\frac{\rho_0}{\rho})/d\varepsilon_0 = 1$, which results in hydrostatic contribution to surface tension. Also, generalized rate $\dot{\mathring{\boldsymbol{\nabla}}}\eta = \boldsymbol{\nabla}\dot{\eta} - \boldsymbol{\nabla}\eta\cdot\boldsymbol{\nabla}\boldsymbol{v}$ (where $\boldsymbol{v}$ is the velocity vector), due to convective term, results in additional gradient-related surface tension. Thus, a physical phenomenon (surface tension) is introduced using simply geometric nonlinearities. In addition to the luck of the idea that the finite-strain theory should be used, the reason why the surface tension theory was not developed before is that the finite-strain theory was just developed in [4]. Introducing the product $\boldsymbol{\nabla}\eta_i\cdot\boldsymbol{\nabla}\eta_j$ allows us to control the

width and energy of the $\mathsf{M}_i - \mathsf{M}_j$ interface independent of $\mathsf{A} - \mathsf{M}_i$ interfaces. This, however, complicates GL Eq. (8) by coupling them through Laplacians. Also, surface tension does not contribute to the driving force for PT directly; rather, it affects the driving force by changing stress distribution. The above equations should be supplemented by the equilibrium equation $\boldsymbol{\nabla} \cdot \boldsymbol{\sigma} = 0$.

Variable surface energy.—Variable surface energy generates the boundary conditions

$$\frac{\rho}{\rho_0} \frac{\partial \psi}{\partial \boldsymbol{\nabla} \eta_i} \cdot \boldsymbol{n} = \frac{\partial \psi^{\nabla}}{\partial \boldsymbol{\nabla} \eta_i} \cdot \boldsymbol{n} = \beta (\nabla \eta_i + b \sum_{j=1, i \neq j}^{n} \boldsymbol{\nabla} \eta_j) \cdot \boldsymbol{n} = -\frac{dq}{d\eta_i}, \tag{10}$$

which generalize known conditions [8] for the 3D case, multiple order parameters, and mixed terms in the gradient energy. Here, $\boldsymbol{n}$ is the normal to the boundary. We assume that in the simplest case $q(\eta_i)$ depends on single "equivalent" order parameter $p = (\sum_{i=1}^{n} \eta_i^2)^{0.5}$. Then, $q(p)$ has the following properties: $q(0) = \gamma_A$; $q(1) = \gamma_M$; $\frac{dq(0)}{dp} = \frac{dq(1)}{dp} = 0$, with γ for the surface energy of phases. The last condition ensures that homogeneous states $\eta_i = 0$ and $\eta_i = 1$ satisfy boundary conditions, which was not the case in previous works [8]. The simplest polynomial expression that satisfies the above condition is $q(p) = \gamma_A + \Delta\gamma[\bar{a}p^2 + (4 - 2\bar{a})p^3 + (\bar{a} - 3)p^4]$, where $\Delta\gamma = \gamma_M - \gamma_A$. It is possible to show that to make a condition of barrierless surface-induced nucleation consistent with a sharp-interface result $\Delta\gamma > E$, where E is interface energy, we need to choose $\bar{a} = 3$. Then $q(p) = \gamma_A + \Delta\gamma(3p^2 - 2p^3)$.

Examples.—We use in the calculations material parameters for cubic to tetragonal PT in NiAl found in [2], $L = 2596.5$ m^2/Ns, $\Delta\gamma = -0.4$ J/m^2, and $b = 0.5$, unless otherwise stated. The FEM approach and code COMSOL were used. For plane stress 2D problems, two M_i are considered with the components of $\boldsymbol{\epsilon}_t$ (0.215, -0.078, -0.078) and (-0.078, 0.215, -0.078). A rectangular sample was considered and quadrilateral and triangle Lagrange elements with quadratic approximation were employed. (1) The effect of b on the energy E_{MM} of $\mathsf{M}_j - \mathsf{M}_i$ interface was studied. Condition $\psi^{\nabla} \geq 0$ implies that $b \leq 1$. We found that $E_{MM} = kE_{AM}$ with $k = 2$ for $b = 0$, $k = 1.523$ for $b = 0.5$, $k = 0.692$ for $b = 0.9$, $k = 0.486$ for $b = 0.95$, and $k = 0$ for $b = 1$. Interface width reduces with the growth of b to zero at $b = 1$. Variation of b changes the nanostructure evolution significantly since it changes the energy balance. (2) For a NiAl single variant, surface-induced nucleation was considered in a 10×10 nm^2 sample for free boundaries and $\theta = 0$ K (see animation 1 in [10]). Surface energy was constant everywhere, excluding a 1 nm part from each side of the x (symmetry) axis at the right-hand boundary. Only half of the sample is considered. For the case with surface tension, a small surface-induced nucleus appeared and reached

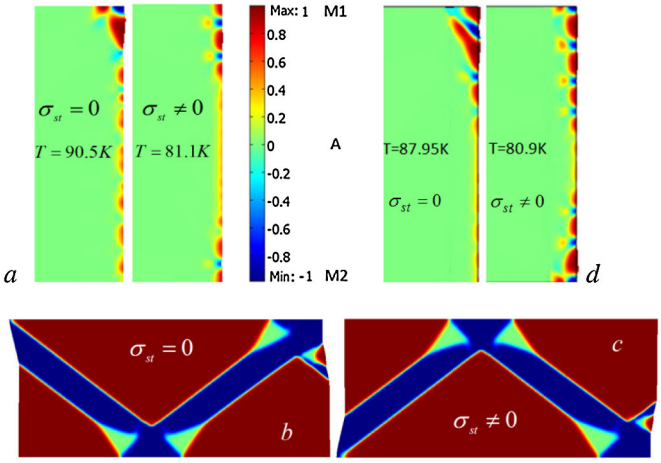

FIG. 1 (color online). Distribution of $\eta_1 - \eta_2$ for the upper part of a 100×100 nm^2 sample and variable surface energy at the right vertical line. (a) At the lowest temperature, when stationary surface-induced nanostructure exists at 90.5 K without surface tension and 81.1 K with surface tension (the 10 nm part of the sample is shown); (b) and (c) stationary nanostructures at 90.5 K for $\boldsymbol{\sigma}_{\rm st} = 0$ and at 81.1 K for $\boldsymbol{\sigma}_{\rm st} \neq 0$; (d) At the lowest temperature, when stationary surface-induced nanostructure exists for $b = 0$ in Eq. (10) at 87.95 K for $\boldsymbol{\sigma}_{\rm st} = 0$ and 80.90 K for $\boldsymbol{\sigma}_{\rm st} \neq 0$.

stationary shape. Without surface tension, PT completes in the entire sample. (3) For two variants and a sample with 100×100 nm^2, the following boundary conditions were applied. Vertical sides are stress-free, zero displacement is applied to the upper horizontal side, and symmetry boundary conditions are used for the x axis. Boundary condition (10) with $\Delta\gamma \neq 0$ is applied to the right vertical line and with $\Delta\gamma = 0$ to other lines. The initial conditions are $\eta_i = 0.001$ and zero stresses in the entire sample. The lowest temperature, when a nontrivial stationary surface-induced nanostructure exists, is 90.5 K without surface tension and 81.1 K with surface tension [Fig. 1(a)] (for $b = 0$ in Eq. (10), it is 87.95 K for $\boldsymbol{\sigma}_{\rm st} = 0$ and 80.90 K for $\boldsymbol{\sigma}_{\rm st} \neq 0$ [Fig. 1(d)], and the transformation path is quite different. At 90.4 K for $\boldsymbol{\sigma}_{\rm st} = 0$ and at 81.0 K for $\boldsymbol{\sigma}_{\rm st} \neq 0$, this nanostructure becomes unstable, and PT spreads in the entire sample with nontrivial path (see animation in [10]).

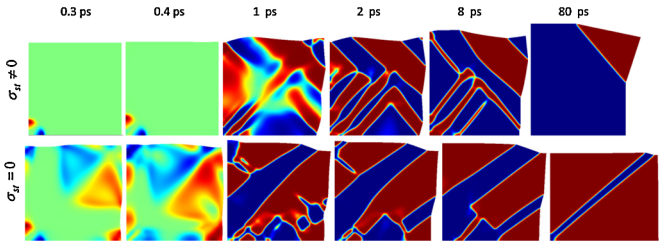

FIG. 2 (color online). Evolution of $\eta_1 - \eta_2$ for preexisting embryo of 2 nm radius with $\eta_i = 0.1$ at the center of a 60×60 nm^2 sample under biaxial tensile stresses of 20 GPa at $\theta = 100$ K with and without surface tension. Quarter of sample is considered.

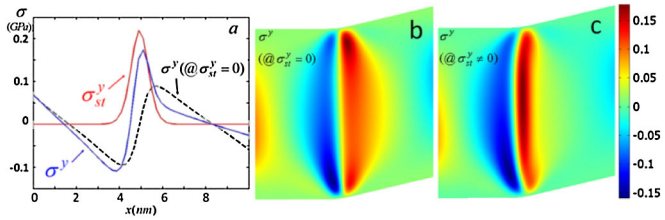

FIG. 3 (color online). (a) Plots of component σ^y_{st} of surface tension, as well as total stress σ^y for the case without and with surface tension, along the line passing through the center of a 10×10 nm^2 sample. (b) and (c) show the distribution of σ^y for the case without and with surface tension, respectively.

A wedge-type nanostructure consisting of two variants propagates from the free surface and forms the stationary solutions, which consist of two intersecting M_2 plates inside a M_1 matrix for $\boldsymbol{\sigma}_{\mathrm{st}} = 0$ and four plates forming a quadrilateral shape for $\boldsymbol{\sigma}_{\mathrm{st}} \neq 0$. Surprisingly, regions of residual A are observed at the intersection of plates, forming a triple junction. Surface tension leads to a curved $\mathsf{A} - \mathsf{M}_2$ interface, change in the width of the M_2 plate, and some other details [Figs. 1(b) and 1(c)]. (5) The evolution of a preexisting embryo of 2 nm radius with $\eta_i = 0.1$ at the center of a 60×60 nm^2 sample under biaxial tensile stresses of 20 GPa at $\theta = 100$ K and $\gamma =$ const everywhere was considered [Fig. 2 and [10]]. The evolution starts with the splitting of the embryo into two martensitic variants separated by austenite. The PT paths for the two cases are completely different. A complex multiconnected nanostructure passes through the coalescence stage and finally ends in a single-variant state that is different for the two cases.

Note that various phenomenological models of coherent interface exist (see review [9]) based on the theory of thin shell and interface constants that are unknown. As a by-product of the current work, we obtained a much more detailed, flexible, and precise model of a coherent interface, which takes into account the heterogeneity of all properties and fields. The importance of finite interface width and surface tension is demonstrated in the example of the $\mathsf{A} - \mathsf{M}$ interface, in which M_1 is rotated by 36.5° to get $\varepsilon^y_t = 0$ [Fig. 3]. For sharp interface we obtained a stress-free solution. For a diffuse interface and $\boldsymbol{\sigma}_{\mathrm{st}} = 0$, even while $\varepsilon^y_t = 0$ everywhere, there is a significant σ^y stress with concentration near the corner. The surface tension σ^y_{st} exceeds this σ^y by a factor of more than 2, and it changes the distribution of σ^y. In general, interface thickness and structure adjust themselves during loading, the interface can appear and disappear, and there are intersecting interfaces, triple junction, and corner points, which are separate problems for the sharp-interface approach.

In summary, GL theory for multivariant PTs is advanced to describe surface tension, $\mathsf{M}_i - \mathsf{M}_j$ interface energy, and variable surface energy in a noncontradictory manner. FEM solutions for surface-induced, pretransformation, barrierless, multivariant nucleation, and the growth of the embryo and nucleus in a nanosize sample allowed us to elucidate the effect of the above contributions. The obtained results also represent an advanced model for coherent interface. Similar developments can be applied for various phenomena involving interfaces, such PTs (liquid-liquid, melting, amorphization, evaporation, electromagnetic, and reconstructive PTs), diffusive PTs described by Cahn-Hilliard theory, twinning, dislocations, fracture, grain growth, and recrystallization, as well as gradient plasticity and damage.

The support of NSF, ARO, DTRA, and ISU, and the help of W. Hong and K. Samani, are acknowledged.

[1] L. Q. Chen, Annu. Rev. Mater. Res. **32**, 113 (2002); J. Slutsker, A. Artemev, and A. L. Roytburd, Acta Mater. **52**, 1731 (2004); Y. Z. Wang and A. G. Khachaturyan, Mater. Sci. Eng. A **438-440**, 55 (2006); W. Zhang, Y. M. Jin, and A. G. Khachaturyan, Acta Mater. **55**, 565 (2007); T. Lookman, A. Saxena, and R. C. Albers, Phys. Rev. Lett. **100**, 145504 (2008).

[2] V. I. Levitas and D. L. Preston, Phys. Rev. B **66**, 134206 (2002); V. I. Levitas and D. L. Preston, Phys. Rev. B **66**, 134207 (2002); V. I. Levitas, D. L. Preston, and D.-W. Lee, Phys. Rev. B **68**, 134201 (2003).

[3] V. I. Levitas and D.-W. Lee, Phys. Rev. Lett. **99**, 245701 (2007); V. I. Levitas, D.-W. Lee, and D. L. Preston, Int. J. Plast. **26**, 395 (2010).

[4] V. I. Levitas, V. A. Levin, K. M. Zingerman, and E. I. Freiman. Phys. Rev. Lett. **103**, 025702 (2009).

[5] A. V. Idesman, J.-Y. Cho, and V. I. Levitas, Appl. Phys. Lett. **93**, 043102 (2008).

[6] V. I. Levitas, A. V. Idesman, and D. L. Preston, Phys. Rev. Lett. **93**, 105701 (2004).

[7] J. Lowengrub and L. Truskinovsky, Proc. R. Soc. A **454**, 2617 (1998); D. M. Anderson, G. B. Fadden, and A. A. Whiller, Physica D (Amsterdam) **151**, 305 (2001).

[8] R. Lipowsky and W. Speth, Phys. Rev. B **28**, 3983 (1983); B. Pluis, D. Frenkel, and J. F. Van der Veen, Surf. Sci. **239**, 282 (1990).

[9] F. D. Fischer *et al.*, Prog. Mater. Sci. **53**, 481 (2008);

[10] See supplementary material at http://link.aps.org/supplemental/10.1103/PhysRevLett.105.165701.